CNS Neuroscience & Therapeutics

ORIGINAL ARTICLE

CNS Neuroscience & Therapeutics

Increase in Neuroexcitability of Unmyelinated C-type Vagal Ganglion Neurons During Initial Postnatal Development of Visceral Afferent Reflex Functions

Zhao Qian,[1] Dong-Jie Liu,[2] Yang Liu,[1] Li-Min Han,[1] Mei Yuan,[1] Jun-Nan Li,[1] Bing Xu,[1] Xiao-Long Lu,[1] Pan-Xiang Cao,[1] Hao-Yan Wang,[3] Xiao-Dong Pan,[3] Li-Juan Wang,[3] Guo-Fen Qiao[1 3] & Bai-Yan Li[1]

1 Department of Pharmacology, Harbin Medical University, Harbin, China
2 Department of Oncology, General Hospital of Da-Qing Oil Field, Da-Qing, China
3 Key Laboratory of Cardiovascular Medicine Research, Ministry of Education, Harbin Medical University, Harbin, China

Keywords
Action potential; Ion channel; Patch-clamp technique; Postnatal development; Visceral afferent.

Correspondence
G.-F. Qiao or B.-Y. Li, Department of Pharmacology, Harbin Medical University, Bao-Jian Road 157, Harbin 150081, China.
Tel.: +86-451-8667-1354;
Fax: +86-451-8669-0493;
E-mails: qiaogf88@163.com.cn or baili@iupui.edu

Received 8 July 2013; revision 22 September 2013; accepted 23 September 2013

doi: 10.1111/cns.12195

SUMMARY

Background: Baroreflex gain increase up closely to adult level during initial postnatal weeks, and any interruption within this period will increase the risk of cardiovascular problems in later of life span. We hypothesize that this short period after birth might be critical for postnatal development of vagal ganglion neurons (VGNs). **Methods:** To evaluate neuroexcitability evidenced by discharge profiles and coordinate changes, ion currents were collected from identified A- and C-type VGNs at different developmental stages using whole-cell patch clamping. **Results:** C-type VGNs underwent significant age-dependent transition from single action potential (AP) to repetitive discharge. The coordinate changes between TTX-S and TTX-R Na^+ currents were also confirmed and well simulated by computer modeling. Although 4-AP or iberiotoxin age dependently increased firing frequency, AP duration was prolonged in an opposite fashion, which paralleled well with postnatal changes in 4-AP- and iberiotoxin-sensitive K^+ current activity, whereas less developmental changes were verified in A-types. **Conclusion:** These data demonstrate for the first time that the neuroexcitability of C-type VGNs increases significantly compared with A-types within initial postnatal weeks evidenced by AP discharge profiles and coordinate ion channel changes, which explain, at least in part, that initial postnatal weeks may be crucial for ontogenesis in visceral afferent reflex function.

Introduction

Vagal ganglion neurons (VGNs) including baroreceptor neurons (BRNs) with cell bodies in the nodose ganglia comprise two major types of neurons with distinct cellular excitability properties and visceral afferent function [1–5]. Myelinated A-type neurons, associated with low threshold and high-frequency discharge including burst firing in response to sudden onset of baroreceptor activity, are more responsible for baroreceptor sensitivity adjustment. In contrast, unmyelinated C-type neurons are associated with high threshold and more tonic discharge, and more responsibility for regulation of mean blood pressure [6–9]. The third subpopulation of VGNs/BRNs classified as myelinated Ah-types based on electrophysiological markers [10] or fast CV has recently been documented in adult female rats [5,11–13]. The neuroexcitability of Ah-types is downregulated by ovariectomy and restored by 17β-estradiol [11,14]. The baroreceptor reflex plays a crucial role in cardiovascular homeostasis by maintaining arterial blood pressure [15]. It has been well documented that the arterial baroreceptor reflex, together with other cardiopulmonary reflexes, undergoes considerable developmental changes during early postnatal period [16,17]. Within the first two postnatal weeks, the baroreflex gain increases nearly 4-fold up closely to adult value [18]. Recent report shows that brain-derived neurotropic factor plays an important role in the functional development of arterial baroreceptor pathways [19]. Any interruption during this critical postnatal period would affect sensory perception and increase the risk of cardiovascular problems in later of life span [20,21]. As first-order neurons, VGNs play key roles in visceral afferent reflex relay, and their neuroexcitability might undergo dramatic changes during the initial postnatal weeks. In this regard, action potential (AP) discharge profiles and underlying ion current changes were evaluated by whole-cell patch performed using identified VGNs isolated from neonatal rats at the ages of postnatal days 1–3 (Pd1–3) or postnatal days 7–10 (Pd7–10), and adult rats. Similar experiment was also conducted on BRNs from adult rats as well. Our

results show that the discharge capability is enhanced significantly, especially seen in unmyelinated C-type VGNs, during this initial postnatal period. This change in neuroexcitability revealed by current-clamp recording is also supported by voltage-clamp and computer modeling study, manifested as corresponding changes in TTX-sensitive and TTX-resistant voltage-gated Na^+ currents, as well as transient and BK (Ca^{2+}-activated, large conductance K^+ channel) currents. More importantly, the developmental changes in neuroexcitability and ionic currents found in this study parallel the postnatal development course of arterial baroreflex gain. It suggests that changes in the Na^+ and K^+ channels in VGNs might be an important mechanism underlying the postnatal increase in arterial baroreflex gain.

Materials and Methods

Drugs and Chemicals

Tetrodotoxin (TTX) and 4-AP were purchased from Sigma (St. Louis, MO, USA). Iberiotoxin (IbTX) was purchased from Alomone laboratories (Jerusalem, Israel). The final concentrations were 1.0 μM for TTX to separate TTX-S and TTX-R Na^+ currents, for isolating transient and BK-KCa K^+ currents, and 5.0 mM 4-AP and 100 nM IbTX were diluted from stocks using recording solutions just before the patch experiments. All toxins and chemicals were applied through bath or local perfusion (~1.0 mL/min). Papain (Sigma), trypsin, type II collagenase, and dispase (Worthington, Lakewood, NJ, USA) were used for enzymatically isolating vagal neurons. The retrograde fluorescent dye (DiI) for aortic depressive nerve (ADN) labeling was purchased from Molecular probe (Eugene, OR, USA). Mg-ATP and Na-GTP (Sigma) were used for preparing pipette solution. All other cell culture agents and chemicals were ordered from Fisher Scientifics or regular sources, otherwise specifically indicated in this section.

Preparation of Isolated Vagal Ganglion Neurons from Neonatal and Adult Rats

Sprague-Dawley rat pups at Pd1–10 and adult males (>250 g) were used for the preparation of isolated VGNs/BRNs in all electrophysiological studies. The procedures for bilateral dissection of neonatal and adult rat vagal ganglia, enzymatic dispersion, and plating of neurons have been previously described in detail [3,4,10]. Briefly, surgical dissection of the vagal ganglia was carried out under stereomicroscopy (×40). The ganglia were immediately placed in chilled support medium containing 90 mL DME-F-12 medium (Sigma), 5 mL fetal bovine serum (HyClone, Logan, UT, USA), 1.0 mL penicillin–streptomycin (Invitrogen, Grand Island, NY, USA), and 100 μM of MITO + Serum Extender (Collaborative Biomedical Products, Bedford, MA, USA). The ganglia were then treated with the same solution by adding 10 units/mL of papain (Sigma) and incubated at 37°C for 20 min. The ganglia were then transferred to the support medium containing 1.0 mg/mL type II collagenase and 2.5 mg/mL dispase (Worthington) and incubated at 37°C for additional 30 min before mechanical dispersion, plating, and incubation of the VGNs/BRNs in support media. Experimental protocols used in this study were approved by the Institutional Animal Care and Use Committee of School of Medical Science, Harbin Medical University.

Fluorescent Labeling and Baroreceptor Neuron Identification

In adult experiment, BRNs from all categories were also investigated, which were identified by the fluorescence first and then further verified by AP characters for the neuron classification. The procedures for fluorescent DiI labeling followed the details as described previously [22]. Briefly, following the anesthesia, the surgical area was shaved, the skin was washed with benzalkonium chloride, and a 2-cm incision was made along the left ventral side of the neck. Under stereomicroscopy, a blunt dissection of the underlying musculature exposed the left carotid artery and surrounding nerve fibers. Under higher magnification, the left ADN, which exclusively contains baroreceptor fibers arising from the aortic arch, was identified. The ADN was separated from the vagus and sympathetic nerves and placed in a 5-mm-long sterile silicon trough. A few crystals of the lipophilic fluorescent dye DiI was placed on the ADN. The nerve, dye crystals, and trough were coated with 0.3 mL of a peripheral nerve encapsulant (Kwik-Sil, WPI). The area was rinsed with sterile saline, and the skin was closed using vicryl suture. The animal fully recovered before returning to the animal facility. At least 3 weeks passed before the animal was considered fully healed and available for experimentation.

Electrophysiological Recordings

The whole-cell patch recordings were performed using MultiClamp 700A or 700B amplifier (Axon Instruments, Union City, CA, USA). Borosilicate glass pipettes (Sutter, Novato, CA, USA) were pulled and polished down to 1.5–2.2 MΩ in normal saline. Following the formation of a gigaohm seal, the pipette capacitance was compensated. The total cell capacitance and electrode access resistance were also compensated, generally to within 60–80% for voltage-clamp study. All patch experiments were performed with proper recording solutions (formula details see Data S1) at room temperature (22–23°C). The recordings were low-pass-filtered to 10 KHz and digitized at 50 KHz. Data collection and analysis were carried out using pCLAMP 10.2 and the Digidata 1440A (Axon Instruments) operating on a PC platform.

Identification of Vagal Ganglion Neurons

Enzymatic dispersion separates the axon from the cell body, and thus, cell types are no longer classified based upon measure of afferent fiber CV. Using an intact ganglion preparation for CV measurement, we recently developed a reliable and robust methodology for classification of an isolated neuron as either a myelinated A-type or an unmyelinated C-type VGNs/BRNs through cluster analysis of a selected set of AP waveform characteristics [5,10] conjugated with visualized microscopic structural characteristics [13]. In addition, the following three parameters were used for identifying the cell type of a particular cell: AP firing

threshold (APFT), AP upstroke velocity measured at 50% peak-to-peak excursion (UV_{APD50}), and AP downstroke velocity (DV_{APD50}), respectively.

Data Acquisition and Analysis

In this experiment, all discharge characters were measured from a single AP elicited by a brief pulse. The repetitive discharge of AP was elicited by depolarization currents in the range from 50 to 300 pA varied according to the cell types. For each tested cell, hyperpolarization current-induced HVS was also evoked by a hyperpolarization current of −120 pA. The resting membrane potentials of vast majority of myelinated and unmyelinated VGNs/BRNs tested in this experiment were below −60 mV, ranging from −59 to −78 mV. For comparison of the neuronal excitability of VGNs/BRNs, small positive current was injected into cells during recordings in the most cases to maintain the RMP at −60 mV. The details with regard to recording protocols of Na^+ and K^+ currents were exactly the same as previously described [10,19,23]. In the present study, all recordings were analyzed using Clampfit (Axon Instruments). Pooled statistics were calculated using Excel (Microsoft, Seattle, WA, USA). Data were expressed as mean ± SD. Comparisons were performed using *t*-test, chi-square test, or ANOVA where appropriate. A *P* value of 0.05 or less was considered statistically significant.

Results

Developmental Changes in Discharge Pattern of Myelinated A-Type and Unmyelinated C-Type Neurons

Compared with C-types, less significant developmental changes in the peak of AP, the duration (APD_{50}), and downstroke velocity (DV_{APD50}) were observed (Table 1) in A-types. APD_{50} became narrower with a faster DV_{APD50} in both Pd7–10 and adult groups. The discharge frequency of tested A-type VGNs/BRNs was increased in Pd7–10 ($P = 0.056$) and adult ($P < 0.05$) groups. By contrast, dramatic developmental changes were observed in either AP waveform or discharge frequency in C-types, manifested by a brief AP duration, lower AP firing threshold (APFT), fast upstroke (UV_{APD50}), and DV_{APD50} along with the age (Table 1). Interestingly, the percentage of repetitive discharge significantly increased during this initial postnatal development (Table S1), a clear transition of single AP to repetitive discharge with significantly reduced stimulus intensity in both Pd7–10 and adult groups ($P < 0.05$ or $P < 0.01$).

Interestingly, the current data indicated significant changes in AP profiles and repetitive discharge properties during development, particularly in unmyelinated C-type VGNs. This phenomenon raises a question of what ion channel mechanisms underlie this developmental change in neuroexcitability during initial postnatal weeks. Based upon the changes in upstroke and downstroke velocity of AP (Table 1), the alternations in current density and voltage-dependent properties of multiple channels, such as voltage-gated Na^+ and K^+ channels, were highly expected. These changes might vary depending upon the cell type.

Developmental Change in Na^+ and K^+ Currents in Myelinated A-type Neurons

Tetrodotoxin-S Na^+ channel is the only Na^+ channel functionally expressed on myelinated A-types. Among all three age groups, the current densities were not altered, and the peaks appeared at −25 mV (Figure 1). Voltage-dependent properties, such as half activation or inactivation voltage ($V_{1/2}$) and slope ($S_{1/2}$) at $V_{1/2}$, were not shifted (Table S2), except for open-state inactivation time constant that was slightly reduced in Pd7–10 and adult than

Table 1 Developmental changes in action potential (AP) discharge characteristics of myelinated A-type and unmyelinated C-type vagal ganglion neurons (VGNs) and baroreceptor neurons (BRNs) in nodose from different age groups. All AP parameters of either A-types or C-types were generated from single AP elicited by a brief pulse, and the maximal frequency of repetitive discharge was determined by suprathreshold step depolarization current injection on the same tested neurons. The average data were expressed by mean ± 1 SD, **P* < 0.05 and ***P* < 0.01 versus Pd1–3

	Myelinated A-type neurons				Unmyelinated C-type neurons			
Parameter	Adult BRNs	Adult VGNs	Pd7–10	Pd1–3	Adult BRNs	Adult VGNs	Pd7–10	Pd1–3
n	7	29	38	41	12	48	51	56
RMP	−62.2 ± 2.9	−63.5 ± 2.3	−62.7 ± 1.30	−62.0 ± 2.9	−62.8 ± 3.8	−62.4 ± 3.3	−63.5 ± 2.21	−63.4 ± 3.7
APFT	−47.4 ± 5.6	−46.3 ± 4.6	−44.4 ± 4.02	−42.6 ± 3.3	−35.2 ± 4.5**	−33.4 ± 4.1**	−31.2 ± 3.4**	−27.0 ± 2.8
$APFF_{MAX}$	−45.7 ± 6.6*	−44 ± 3.6*	−33.4 ± 4.02	−28.1 ± 3.6	9.1 ± 2.4**	7.2 ± 1.6**	5.4 ± 1.5**	1.52 ± 0.3
APD_{50}	0.72 ± 0.08*	0.75 ± 0.12*	0.78 ± 0.19*	0.88 ± 0.12	2.12 ± 0.7**	2.24 ± 0.4**	2.42 ± 0.7**	3.31 ± 0.8
AP_{PEAK}	56.8 ± 2.3**	55.4 ± 4.3**	51.2 ± 3.5*	40.6 ± 3.4	56.7 ± 3.6**	58.4 ± 2.9**	54.6 ± 3.0**	45.7 ± 3.7
AHP_{PEAK}	−65.3 ± 0.89	−66.0 ± 1.19	−65.6 ± 1.26	−65.1 ± 1.32	−64.8 ± 2.11	−66.2 ± 3.1	−65.5 ± 2.7	−65.4 ± 3.4
AHP_{80}	22.6 ± 7.8	26.7 ± 9.8	28.7 ± 10.4	29.4 ± 14.6	83.3 ± 20.7	78.8 ± 18.5	75.1 ± 24.1	89.4 ± 29.4
UV_{APD50}	244 ± 31	238 ± 24	241 ± 19	211 ± 26	95.3 ± 25.7**	93.3 ± 22.4**	85.8 ± 19.1*	55.6 ± 23.7
DV_{APD50}	−197 ± 27**	−191 ± 19**	−178 ± 24**	−114 ± 12	−51.6 ± 7.2**	−49.3 ± 6.5**	−43.6 ± 5.9*	−27.3 ± 5.3

RMP, Resting membrane potential (mV); APFT, AP firing threshold (mV); APFF, AP firing frequency (Hz); APD_{50}, AP duration at 50% deflection (ms); AP_{Peak}, AP peak (mV); AHP_{Peak}, peak deflection after hyperpolarization (mV); AHP_{80}, time for 80% recovery to RMP after AHP (ms); UV_{APD50}, upstroke velocity at APD_{50} (mV/ms); DV_{APD50}, downstroke velocity at APD_{50} (mV/ms).

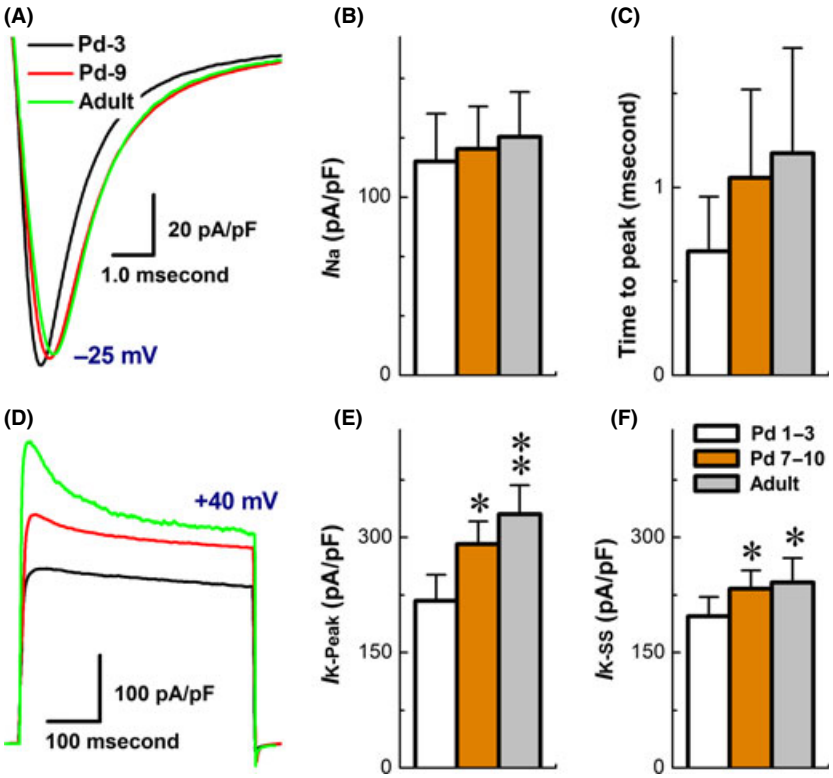

Figure 1 Developmental change in ion channel current recorded from myelinated A-type vagal ganglion neurons (VGNs) and baroreceptor neurons (BRNs). Voltage-clamp recordings were performed on myelinated A-type vagal ganglion neurons isolated from Pd1–3, Pd7–10, and adult rats, respectively. (**A**) the representative traces of TTX-sensitive Na^+ currents from P3, P10, and adult rats. The cell was held at −80 mV and stepped from −70 mV to +40 mV with 5 mV increment, 60 ms duration, and 1.0 second step interval. (**B**) The representative traces of total K^+ currents and transient component/4-AP-sensitive K^+ currents from P3, P10, and adult rats. The cell was held at −80 mV and increased from −70 mV to +40 mV with 5 mV increment, 400 ms duration, and 1.0 second step interval. 4-AP-sensitive component of K^+ currents were subtracted from the currents remaining in the presence of 5.0 mM of 4-AP from the total K^+ currents. (**C,D**) The average data in current density and inactivation time constant of TTX-sensitive Na^+. (**E,F**) The average data in current density of K^+ currents measured at peak and steady status (SS). The average data were presented as mean ± SD, n = 7–14 recordings. *$P < 0.05$ and **$P < 0.01$ versus Pd1–3.

Pd1–3 group ($P < 0.05$, data not shown). In addition, larger total K^+ currents were observed in A-types, and the current density measured at peaks was increased dramatically compared with steady status (SS) during development (Figure 1), suggesting an age-dependent increase in transient component of K^+ currents. With these corresponding changes in TTX-S Na^+ and transient K^+ components, slight changes in discharge profiles in A-types are highly expected along initial postnatal weeks (Table S1).

Developmental Change in TTX-S and TTX-R Na^+ Currents in Unmyelinated C-type Neurons

Compared with myelinated A-types, significant developmental changes in discharge profiles were observed in C-types (Table 1). In this regard, voltage-dependent Na^+ currents were recorded from three age groups, and TTX-S and TTX-R components were separated by 1.0 μM TTX (Figure 2A–C). The results showed that even though the total current density (TTX-S + TTX-R, black traces) was not changed among groups, but TTX-R Na^+ component (red traces) was tremendously increased ($P < 0.01$) in adult and Pd7–10 than Pd1–3 group (Figure 2D). The ratios (%) of TTX-R/TTX-S + TTX-R were increased from 21.4 ± 19.4% in Pd1–3 to 72.7 ± 32.5% in Pd7–10 ($P < 0.01$) and 87.7 ± 31.5% ($P < 0.01$) in adult rats. The total charges of Na^+ ion flowing through the activated channels were almost doubled ($P < 0.01$) in Pd7–10 and adult compared with Pd1–3 group (Figure 2E). As developmental changes in TTX-R component, the peaks were shifted to more depolarized direction. The time to peaks was increased in age-dependent fashion (Figure 2F), and the voltage-dependent profiles were rightward-shifted (Table S2) with marked reduction in open-state inactivation time constants (tau1 and tau2) of total Na^+ currents (Figure 2G).

Developmental Change in Total K^+ Currents and Transient Component in Unmyelinated C-type Neurons

The transient (4-AP-sensitive or $I_A + I_D$) of outward K^+ currents is a key player in regulating neuroexcitability and discharge pattern of VGNs/BRNs. Therefore, total K^+ currents and 4-AP-sensitive

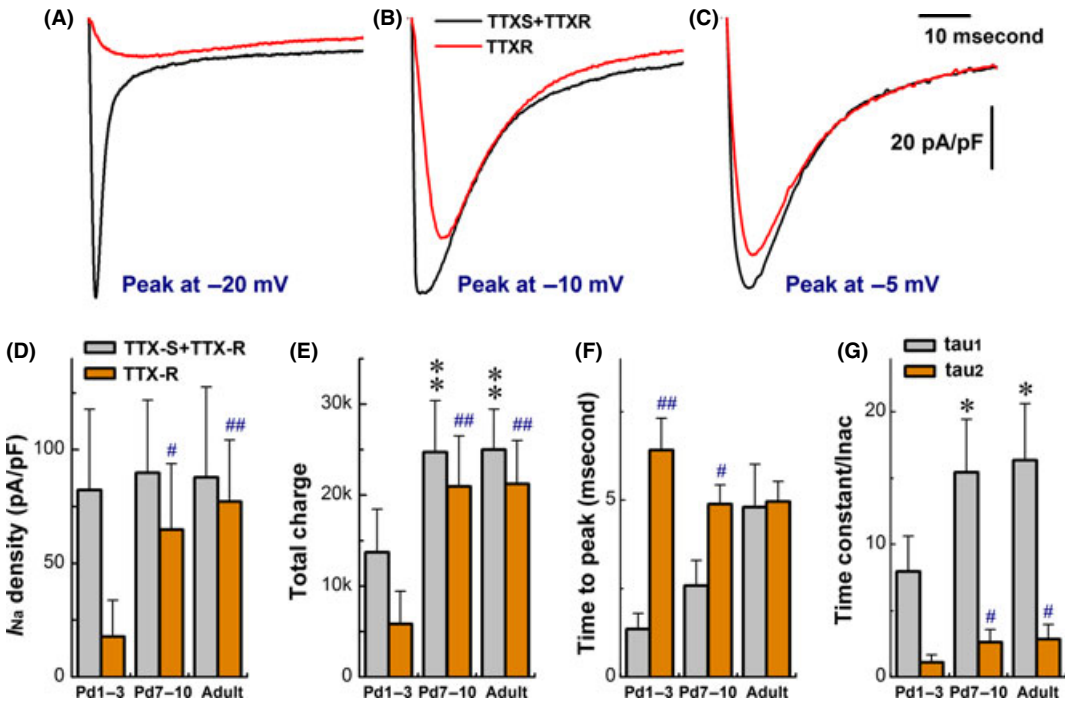

Figure 2 Coordinated change in TTX-sensitive (TTX-S) and TTX-resistant (TTX-R) Na^+ currents of unmyelinated C-type vagal ganglion neurons (VGNs) and baroreceptor neurons (BRNs) during the development. Voltage-clamp recordings were performed on unmyelinated VGNs/BRNs isolated from Pd1–3, Pd7–10, and adult rats, respectively. The cell was held at −80 mV and increased from −70 mV to +40 mV with 5 mV increment, 60 ms duration, and 1.0 second step interval. TTX-R Na^+ current was isolated by subtracting the current remaining in the presence of 1.0 μM of TTX from total Na^+ currents. (**A**–**C**) The representative traces of total Na^+ currents (black) and TTX-R components (red) from Pd-3, Pd-9, and adult rats, respectively. (**D**) Changes in current density. (**E**) Changes in total charge passing through channels. (**F**) Changes in time to peaks. (**G**) Changes in inactivation time constant (tau value) best described by two exponential fitting. The average data were presented as mean ± SD, n = 7–14 recordings. *$P < 0.05$ and **$P < 0.01$ versus Pd1–3 for total Na^+ currents. $^{\#}P < 0.05$ and $^{\#\#}P < 0.01$ versus Pd7–10 for TTX-R components. Scale bars in (**C**) also applied for (**A**) and (**B**).

components were investigated from all age groups (Figure 3A–C). Averaged data showed that the normalized peak of total K^+ currents was identical (Fig. 3D), but the remarkable trend of increases in 4-AP-sensitive components was observed during development ($P < 0.05$ or $P < 0.01$), and the percentage of 4-AP-sensitive I_A (rapid inactivation) and I_D (slow inactivation) components calculated based on total K^+ currents were 24.9 ± 9.39% and 21.3 ± 8.56% in Pd1–3 (n = 6); 49.8 ± 10.0% and 40.35 ± 8.66% in Pd7–10 (n = 6); and 75.7 ± 12.4% and 52.7 ± 10.6% in adult (n = 7) groups. The ratio of I_A versus I_D was also dramatically enhanced from 1.175 for Pd1–3 to 1.233 for Pd7–10 and 1.438 for adult VGNs. Although total current density was not altered, the total charges (Fig. 3E) flowing through the activated K^+ channels were declined ($P < 0.05$ or $P < 0.01$) during the development, while the total charges for 4-AP-sensitive ($I_A + I_D$) components were increased in either Pd7–10 ($P < 0.05$) or adult ($P < 0.01$) group.

Effects of 4-AP on Action Potential and Discharge Pattern of Unmyelinated C-type Neurons

4-AP-sensitive K^+ component modulates AP profiles and repetitive discharge [24–27]. To verify whether the overall changes in 4-AP-sensitive component (Fig. 3) impact on neuronal developmental change in neuroexcitability, a brief pulse- and step depolarization-elicited APs in C-type VGNs were recorded in all groups with and without 5 mM 4-AP. Averaged data indicated that APD_{50} reduced during development, consistent well with previous recordings (Table 1 and Figure S1), whereas it was dramatically prolonged in the presence of 4-AP by 46% in Pd7–10 ($P < 0.01$) and 49% in adult ($P < 0.01$), respectively, compared with 24% in Pd1–3 VGNs. By blocking transient K^+ component, the firing frequency was also dramatically increased ($P < 0.01$, Table 2) in all age groups, particularly in Pd7–10 and adults from single or burst AP without increasing the stimulus intensity.

Effects of Iberiotoxin on Action Potential and Discharge Pattern of Unmyelinated C-type Neurons

BK-KCa is another critical contributor to repolarization phase of AP in sensory neurons and closely impacts on the modulation of neuroexcitability and neurotransmission [28]. To elucidate the contribution of BK-KCa, similar sets of current-clamp recordings with 100 nM IbTX were conducted in identified C-types. Intriguingly, APD_{50} was prolonged by more than 60% in Pd1–3, but only less than 20% of widening was confirmed in Pd7–10 and adult

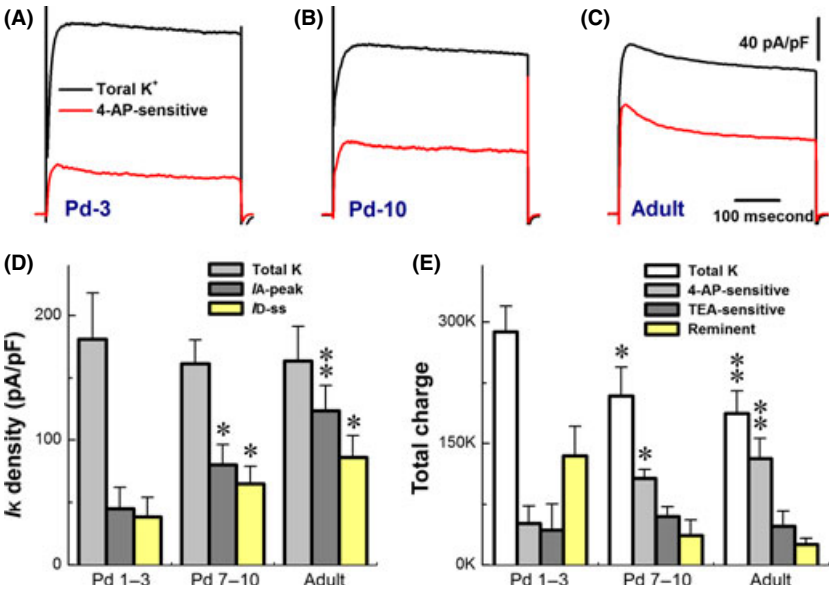

Figure 3 Developmental changes in total K^+ currents and transient/4-AP-sensitive component of unmyelinated C-type vagal ganglion neurons (VGNs) and baroreceptor neurons (BRNs). Voltage-clamp recordings were performed on unmyelinated C-type VGNs/BRNs isolated from Pd1–3, Pd7–10, and adult rats, respectively. The cell was held at −80 mV and increased from −70 mV to +40 mV with 5 mV increment, 400 ms duration, and 1.0 second step interval. The 4-AP-sensitive component of K^+ currents was isolated by the subtraction of currents remained in the presence of 5.0 mM of 4-AP from total K^+ currents. (**A–C**) The representative traces of total K^+ currents (Black) and 4-AP-sensitive components (Red) from Pd1–3, Pd7–10, and adult, respectively. (**D**) Changes in current density. (**E**) Changes in total charges passing through channels. The average data were presented as mean ± SD, n = 9–16 recordings. *$P < 0.05$ and **$P < 0.01$ versus Pd1–3 in all cases. The scales bars in (**B**) and (**C**) also apply for others.

Table 2 Effects of 4-AP and iberiotoxin (IbTX) on action potential (AP) and firing frequency in unmyelinated C-type vagal ganglion neurons isolated from Pd1–3, Pd7–10, and adult rats. Single AP and repetitive firings (Hz) were evoked by brief pulse and step depolarization, respectively, before and after 4-AP or IbTX. Average data were expressed as mean ± SD. *$P < 0.05$ and **$P < 0.01$ versus control

	5.0 mM 4-AP, n = 6		100 nM IbTX, n = 7	
Groups	Control	Test	Control	Test
Pd1–3	1.12 ± 0.23	5.01 ± 1.4*	1.07 ± 0.32	3.02 ± 0.41*
Pd7–10	1.45 ± 0.58	8.6 ± 3.1**	1.39 ± 0.37	13.6 ± 2.1**
Adult	1.94 ± 0.81	d10.3 ± 4.4**	1.66 ± 0.65	15.6 ± 3.4**

C-types ($P < 0.01$). The corresponding changes in DV_{APD50} were also observed, respectively. For further testing effect of IbTX on discharge profile, threshold step depolarization was selected in control and test recordings. Results showed that 100 nM IbTX induced repetitive discharges in all tested C-type VGNs of each group, and the firing frequency in the presence of IbTX was significantly increased ($P < 0.01$) to 3.02 ± 0.41 Hz in Pd1–3, 13.6 ± 2.1 Hz in Pd1–7, and 15.6 ± 3.4 Hz in adult VGNs (Table 2).

Ontogenesis of BK-type Ca^{2+}-Activated K^+ (BK_{Ca}) Currents in Unmyelinated C-type Neurons

Based on our current-clamp data with IbTX, the developmental reductions in functional expression of BK-KCa are highly expected. To further confirm this observation, IbTX-sensitive currents were isolated (Figure 4B), and results indicated that the current density of IbTX-sensitive component was more than 2-fold larger in Pd1–3 (86.9 ± 18.6 pA/pF) than those observed in Pd7–10 (43.4 ± 9.1 pA/pF, $P < 0.01$) and adult (40.7 ± 6.9 pA/pF, $P < 0.01$) C-types without alternation of total K^+ current density. The current–voltage relationship (I-V curve) showed that the activation voltage was at least 5 mV more depolarized in Pd1–3 (~-25 mV) than those in Pd7–10 (~−35 mV) and adult (~−40 mV) groups (Figure 4C).

Discussion

Vagal ganglion neurons in the nodose, for example, baroreceptor neurons (BRNs, the first-order neurons of baroreflex), process and encode mechanosensitive information by generating sequences of APs [29]. It has long been known that AP spike is initiated and shaped by several voltage-gated ion channel currents, like voltage-gated Na^+, K^+, and Ca^{2+} currents and their subtypes. Any one of them changed during initial postnatal weeks, the coordinative changes in AP waveshape would be expected, and the neuroexcitability would be modulated, paralleled with those changes [30–34]. Our previous data demonstrate that VGNs/BRNs functionally express all major voltage-gated ion channels [25,35–37] that are involved in regulation of neuroexcitability [37,38]. However, little is known regarding neuroexcitability change and underlying ion channel mechanisms during initial postnatal development, particularly the changes within the first two postnatal weeks. That may better

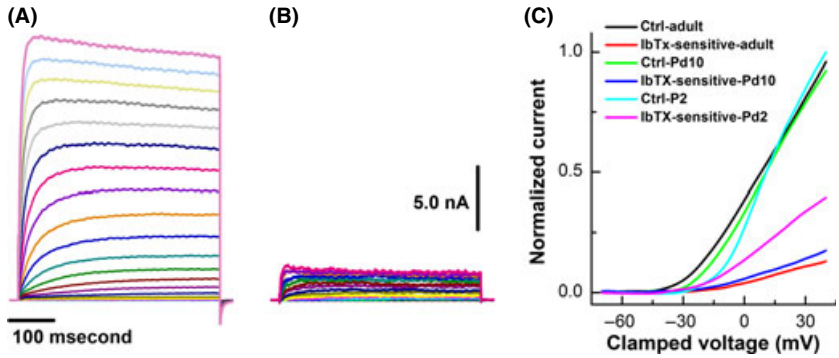

Figure 4 Effects of 100 nM iberiotoxin (IbTX) on BK-type Ca^{2+}-activated K^+ (BK-KCa) currents of unmyelinated C-type vagal ganglion neurons (VGNs) and baroreceptor neurons (BRNs) isolated from Pd1–3, Pd7–10, and adult rats. C-type VGNs/BRNs were identified by the action potential waveform characters conjugated with the repolarization "hump" just before the voltage-clamp recordings. After complete bath perfusion with extracellular K^+ recording solution, the whole-cell K^+ currents were recorded with holding potential of −80 mV and the depolarization stepped from −70 to +40 mV with 400 ms duration and 5 mV increments. (**A**) The representative K^+ currents recorded from unmyelinated C-types BRNs of adult rats; (**B**) IbTX-sensitive component of K^+ currents were subtracted from the remaining portion in the presence of 100 nM IbTX from total K^+ currents shown in (**A**); (**C**) The current–voltage relationships (I-V curve) of total K^+ and IbTX-sensitive components from unmyelinated C-type VGNs/BRNs of different age groups. Scale bars in (**A**) or (**B**) also apply for all.

explain why the baroreflex gain upregulates during this typical window.

Ontogenesis of Myelinated A-type Vagal Ganglion Neurons

Myelinated A- and unmyelinated C-type VGNs/BRNs play different roles in visceral afferent reflex. By looking at repetitive discharge capability, unlike C-types, the obvious increase in firing frequency was only observed in adult rats, suggesting that this developmental formation of myelination in A-type neurons may be the key for this delayed postnatal change [39,40] compared with unmyelinated C-type neurons. Additionally, the facts that mean BP increases up closely to adult level during initial postnatal life and unmyelinated C-types are more important for regulation of mean blood pressure [6–9] support the notion that myelinated A-type neurons may play a less role in early postnatal development of visceral afferent reflex function and baroreflex gain during initial postnatal weeks.

Ontogenesis of Unmyelinated C-type Vagal Ganglion Neurons

Compared with A-types, C-type neurons undergo dramatic postnatal changes in discharge profiles and show a clear transition from single/burst AP in Pd1–3 to repetitive discharge with less stimulation required in older rats. Analyzed current-clamp data demonstrate that the features related to neuroexcitability such as APFT, UV_{APD50}, and DV_{APD50} (Table 1) are significantly shifted toward more excitable direction during postnatal development. Thus, coordinative change in channel/s underlying this functional alternation in unmyelinated C-type VGNs/BRNs is highly expected.

The alternation of APFT and UV_{APD50} in C-types strongly implies that either current density or voltage-dependent properties of Na^+ channels may change during initial postnatal life. The present study clearly demonstrates that the ratios of TTX-R/TTX-S+TTX-R and TTX-R components were significantly increased in Pd7–10 to an identical level of adult group, whereas the current density of total Na^+ currents remained unchanged, suggesting a coordinate change between TTX-S and TTX-R Na^+ channels, and consequently enhances the neuroexcitability, which is further supported by our computer modeling study (Figures S2–S4). TTX-S Na^+ channel is more responsible for setting APFT and [28,37]. Even though the current density is reduced during postnatal development, more negative APFT may require less Na^+ channel activation to accelerate membrane potential to the activation window. TTX-R Na^+ currents contribute to AP repolarization [37,41], particularly the formation of repolarization hump (Figure S3), and closely impact on the repetitive discharge capability [37]. Our data clearly demonstrate that the increase in the frequency of repetitive discharge parallels well with the increase in TTX-R Na^+ components and GNa1 in computer simulation (Figure S4) because the reactivation rate of TTX-R Na^+ channels is more than 10-fold faster compared with TTX-S Na^+ channels [37]. Additionally, although neonatal C-types express large proportion of TTX-S Na^+ components compared with adult group, only <20% of TTX-S Na^+ channels are available at near resting membrane potential (RMP) [37]. However, the availability of TTX-S Na^+ channels in adult rat is about 50–60% of total near RMP because the $V_{1/2}$ of inactivation for both TTX-S and TTX-R Na^+ currents in adult VGNs/BRNs occurred at more depolarized voltage than that of activation on neonatal; therefore, the activation window becomes larger in adult compared with neonatal rats [35], which means that the more Na^+ channels within activation window are opened dynamically, resulting in postnatal upregulation in neuroexcitability of C-types. The postnatal change in TTX-R is consistent with molecular evidence that the expression of Nav1.8 (TTX-R component) increases with age and reaches adult levels by postnatal day 7 [42].

Among voltage-gated K^+ channels, both transient 4-AP-sensitive K^+ ($I_A + I_D$) [24,43] and BK-KCa (IbTX-sensitive)

[24,25,38,44,45] play critical roles in shaping AP waveform over the course of repolarization and neuroexcitability. Our voltage-clamp data indicate that the current density of total K^+ currents in C-types was not changed, but 4-AP-sensitive K^+ component and the ratio of I_A versus I_D enhanced coordinately with the reduction in IbTX-sensitive K^+ currents over the course of postnatal development. These results demonstrated that transient 4-AP-sensitive component may play more important roles to shape AP in later postnatal stage. These data also suggested that the increase in transient K^+ component may be compensated by the loss of BK-KCa currents along initial postnatal weeks. This coordinative change in transient K^+ and BK-KCa components may contribute, at least in part, to maintain the firing capability and the transition from single AP to repetitive discharge over the course of the development.

Clinical Relevance

Increasing evidence demonstrates that initial postnatal weeks are critical for the postnatal development of visceral afferent reflex function, such as baroreflex and cardiopulmonary reflex. Early-life stressors that may program blood pressure control mechanisms and modify the adaptation process of cardiopulmonary reflex will definitely increase the risk of cardiovascular (hypertension) [46,47], pulmonary (COPD and asthma) [48], and cardiometabolic diseases (obesity and type II diabetes) [49] in later life. The efficient and high afferent reflex gain observed in this short period after birth may play an important role in preventing or attenuating increases in cardiovascular and cardiopulmonary systems in response to pathophysiological stresses. Modifications of early postnatal development will have important implications for future risks throughout life. This view represents a fundamental change in current pathophysiological and therapeutic concepts and holds the potential to develop novel preventative and therapeutic strategies. However, for the successful development of such approaches, a clear understanding of underlying mechanisms of early postnatal development in visceral afferent reflex function and the validation of relevant preclinical models are keys to facilitate translational research.

Conclusion

These data demonstrate for the first time that ion channel coordination between voltage-gated Na^+ and K^+ channels and their subtypes contributes largely to initial postnatal development of neuroexcitability, especially in unmyelinated C-type neurons. These data also provide a novel insight into underlying ion channel mechanisms of afferent reflex gain within the first two postnatal weeks.

Acknowledgments

This project was supported by research grants from Chinese Natural Science Foundation (30973532; 81173051; 31171122) and Education Department (20112307110008).

Conflict of Interest

The authors declare no conflict of interest.

References

1. Schild JH, Kunze DL. Differential distribution of voltage-gated channels in myelinated and unmyelinated baroreceptor afferents. *Auton Neurosci* 2012;**172**:4–12.
2. Schild JH, Clark JW, Hay M, et al. A- and C-type rat nodose sensory neurons: model interpretations of dynamic discharge characteristics. *J Neurophysiol* 1994;**71**:2338–2358.
3. Li BY, Schild JH. Patch clamp electrophysiology in nodose ganglia of adult rat. *J Neurosci Methods* 2002;**115**:157–167.
4. Li BY, Schild JH. Comparisons of somatic action potentials from dispersed and intact rat nodose ganglia using patch-clamp technique. *Acta Pharmacol Sin* 2002;**23**:481–489.
5. Li BY, Qiao GF, Feng B, et al. Electrophysiological and neuroanatomical evidence of sexual dimorphism in aortic baroreceptor and vagal afferents in rat. *Am J Physiol Regul Integr Comp Physiol* 2008;**295**:R1301–R1310.
6. Chapleau MW, Abboud FM. Determinants of sensitization of carotid baroreceptors by pulsatile pressure in dogs. *Circ Res* 1989;**65**:566–577.
7. Chapleau MW, Hajduczok G, Abboud FM. Pulsatile activation of baroreceptors causes central facilitation of baroreflex. *Am J Physiol* 1989;**256**:H1735–H1741.
8. Seagard JL, Hopp FA, Drummond HA, et al. Selective contribution of two types of carotid sinus baroreceptors to the control of blood pressure. *Circ Res* 1993;**72**:1011–1022.
9. Brooks VL, Sved AF. Pressure to change? Re-evaluating the role of baroreceptors in the long-term control of arterial pressure. *Am J Physiol Regul Integr Comp Physiol* 2005;**288**:R815–R818.
10. Li BY, Schild JH. Electrophysiological and pharmacological validation of vagal afferent fiber type of neurons enzymatically isolated from rat nodose ganglia. *J Neurosci Methods* 2007;**164**:75–85.
11. Qiao GF, Li BY, Lu YJ, Fu YL, Schild JH. 17Beta-estradiol restores excitability of a sexually dimorphic subset of myelinated vagal afferents in ovariectomized rats. *Am J Physiol Cell Physiol* 2009;**297**:C654–C664.
12. Qiao GF, Qian Z, Sun HL, et al. Remodeling of hyperpolarization-activated current, Ih, in Ah-type visceral ganglion neurons following ovariectomy in adult rats. *PLoS ONE* 2013;**8**:e71184.
13. Lu XL, Xu WX, Yan ZY, et al. Subtype identification in acutely dissociated rat nodose ganglion neurons based on morphologic parameters. *Int J Biol Sci* 2013;**9**:716–727.
14. Guyenet PG. The sympathetic control of blood pressure. *Nat Rev Neurosci* 2006;**7**:335–346.
15. Tsyrlin VA, Galagudza MM, Kuzmenko NV, et al. Arterial baroreceptor reflex counteracts long-term blood pressure increase in the rat model of renovascular hypertension. *PLoS ONE* 2013;**8**:e64788.
16. Dutschmann M, Morschel M, Rybak IA, et al. Learning to breathe: control of the inspiratory-expiratory phase transition shifts from sensory- to central-dominated during postnatal development in rats. *J Physiol* 2009;**587**:4931–4948.
17. Waki H, Yamasaki M, Katahira K, et al. Developmental changes in functional characteristics of aortic baroreceptor afferents in rats. *Exp Physiol* 2008;**93**:319–324.
18. Ishii T, Kuwaki T, Masuda Y, et al. Postnatal development of blood pressure and baroreflex in mice. *Auton Neuronsci* 2001;**94**:34–41.
19. Martin JL, Jenkins VK, Hsieh HY, et al. Brain-derived neurotrophic factor in arterial baroreceptor pathways: implications for activity-dependent plasticity at baroafferent synapses. *J Neurochem* 2009;**108**:450–464.
20. Chu YC, Yang CC, Lin HT, et al. Neonatal nociception elevated baseline blood pressure and attenuated cardiovascular responsiveness to noxious stress in adult rats. *Int J Dev Neurosci* 2012;**30**:421–426.
21. Gough A, Linden M, Spence D, Patterson CC, Halliday HL, McGarvey LP. Impaired lung function and Health Status in Adult Survivors of Bronchopulmonary Dysplasia. *J Eur Respir* 2013; doi: 10.1183/09031936.00039513 [Epub ahead of print].
22. Qiao GF, Cheng ZF, Huo R, et al. GM1 ganglioside contributes to retain the neuronal conduction and neuronal excitability in visceral and baroreceptor afferents. *J Neurochem* 2008;**106**:1637–1645.
23. Matsumoto S, Yoshida S, Ikeda M, et al. Effects of acetazolamide on transient K+ currents and action potentials in nodose ganglion neurons of adult rats. *CNS Neurosci Ther* 2011;**17**:66–79.
24. Segal M, Rogawski MA, Barker JL. A transient potassium conductance regulates the excitability of cultured hippocampal and spinal neurons. *J Neurosci* 1984;**4**:604–609.
25. Glazebrook PA, Ramirez AN, Schild JH, et al. Potassium channels Kv1.1, Kv1.2 and Kv1.6 influence excitability of rat visceral sensory neurons. *J Physiol* 2002;**541**:467–482.
26. Iwasaki S, Nakajima T, Chihara Y, et al. Developmental changes in the expression of Kv1 potassium channels in rat vestibular ganglion cells. *Brain Res* 2012;**1429**:29–35.
27. Nakamura Y, Takahashi T. Developmental changes in potassium currents at the rat calyx of Held presynaptic terminal. *J Physiol* 2007;**581**:1101–1112.
28. Li BY, Glazebrook P, Kunze DL, et al. KCa1.1 channel contributes to cell excitability in unmyelinated but not

myelinated rat vagal afferents. *Am J Physiol Cell Physiol* 2011;**300**:C1393–C1403.
29. Li B, Schild JH. Persistent tetrodotoxin-resistant Na+ currents are activated by prostaglandin E2 via cyclic AMP-dependent pathway in C-type nodose neurons of adult rats. *Biochem Biophys Res Commun* 2007;**355**:1064–1068.
30. Rothe T, Juttner R, Bahring R, et al. Ion conductances related to development of repetitive firing in mouse retinal ganglion neurons in situ. *J Neurobiol* 1999;**38**:191–206.
31. Huguenard JR, Hamill OP, Prince DA. Developmental changes in Na+ conductances in rat neocortical neurons: appearance of a slowly inactivating component. *J Neurophysiol* 1988;**59**:778–795.
32. Skaliora I, Robinson DW, Scobey RP, et al. Properties of K+ conductances in cat retinal ganglion cells during the period of activity-mediated refinements in retinofugal pathways. *Eur J Neurosci* 1995;**7**:1558–1568.
33. Kressin K, Kuprijanova E, Jabs R, et al. Developmental regulation of Na+ and K+ conductances in glial cells of mouse hippocampal brain slices. *Glia* 1995;**15**:173–187.
34. Bordey A, Sontheimer H. Postnatal development of ionic currents in rat hippocampal astrocytes in situ. *J Neurophysiol* 1997;**78**:461–477.
35. Huang SJ, Robinson DW. Activation and inactivation properties of voltage-gated calcium currents in developing cat retinal ganglion cells. *Neurosci* 1998;**85**:239–247.
36. Schild JH, Kunze DL. Experimental and modeling study of Na+ current heterogeneity in rat nodose neurons and its impact on neuronal discharge. *J Neurophysiol* 1997;**78**:3198–3209.
37. Li BY, Schild JH. Correlation between the activation and inactivation gating profiles of the TTX-resistant Na+ current from fluorescently identified aortic baroreceptor neurons of the adult rat. *FASEB J* 2005;**19**(Suppl.):A606.
38. Li BY, Feng B, Tsu HY, et al. Unmyelinated visceral afferents exhibit frequency dependent action potential broadening while myelinated visceral afferents do not. *Neurosci Lett* 2007;**421**:62–66.
39. Yamasaki M, Matsumoto S, Shimizu T. Postnatal development of the rat aortic nerve. *Jpn J Physiol* 1995;**45** (Suppl.):S240.
40. Yamasaki M, Shimizu T, Kanno T, et al. Postnatal change of the number of myelinated fibers in the rat aortic nerve. *Jpn J Physiol* 1996;**46** (Suppl.):S197.
41. Stansfeld CE, Wallis DI. Properties of visceral primary afferent neurons in the nodose ganglion of the rabbit. *J Neurophysiol* 1985;**54**:245–260.
42. Blair NT, Bean BP. Roles of tetrodotoxin (TTX)-sensitive Na+ current, TTX-resistant Na+ current, and Ca2+ current in the action potentials of nociceptive sensory neurons. *J Neurosci* 2002;**22**:10277–10290.
43. Benn SC, Costigan M, Tate S, et al. Developmental expression of the TTX-resistant voltage-gated sodium channels Nav1.8 (SNS) and Nav1.9 (SNS2) in primary sensory neurons. *J Neurosci* 2001;**21**:6077–6085.
44. Zhang XF, Gopalakrishnan M, Shieh CC. Modulation of action potential firing by iberiotoxin and NS1619 in rat dorsal root ganglion neurons. *Neurosci* 2003;**122**:1003–1011.
45. Li W, Gao SB, Lv CX, et al. Characterization of voltage-and Ca2 + -activated K+ channels in rat dorsal root ganglion neurons. *J Cell Physiol* 2007;**212**:348–357.
46. Yu JG, Zhou RR, Cai GJ. From hypertension to stroke: mechanisms and potential prevention strategies. *CNS Neurosci Ther* 2011;**17**:577–584.
47. Liu AJ, Zang P, Guo JM, et al. Involvement of acetylcholine-alpha7nAChR in the protective effects of arterial baroreflex against ischemic stroke. *CNS Neurosci Ther* 2012;**18**:918–926.
48. Leynaert B, Sunyer J, Garcia-Esteban R, et al. Gender differences in prevalence, diagnosis and incidence of allergic and non-allergic asthma: a population-based cohort. *Thorax* 2012;**67**:625–631.
49. Nihalani N, Schwartz TL, Siddiqui UA, Megna JL. Obesity and psychotropics. *CNS Neurosci Ther* 2012;**18**:57–63.

Supporting Information

The following supplementary material is available for this article:

Data S1. Formula for recoding solution.
Figure S1. Developmental changes in action potentials and discharge profiles of myelinated A- (upper panel) and unmyelinated C-type (lower panel) VGNs isolated from postnatal day 3, day 9 and adult rats.
Figure S2. Computer modeling study of coordinative changes of TTX-S and TTX-R Na^+ channel component during postnatal development.
Figure S3. Computer simulations of action potential hump during repolarization by modification of TTX-R Na^+ currents.
Figure S4. Computer modeling data demonstrate that TTX-R Na^+ currents are more responsible for repetitive discharge capability during postnatal development.
Table S1. Differential discharge patterns of action potential (AP) in myelinated A-type and unmyelinated C-type vagal ganglion neurons (VGNs) and baroreceptor neurons (BRNs) from different age groups.
Table S2. Developmental changes in Voltage-dependent properties of voltage-gated Na^+ channels recorded from myelinated A-type (left panel) and unmyelinated C-type VGNs and BRNs (right panel) with different age groups.

